Weierstraß-Institut
für Angewandte Analysis und Stochastik

im Forschungsverbund Berlin e.V.

Plasma induced pulse breaking in filamentary self-compression

Carsten Brée [1,2], Ayhan Demircan[1], Stefan Skupin[3,4], Luc Bergé[5]

and Günter Steinmeyer[,2,6]

[1]   Weierstrass Institute for Applied Analysis and Stochastics, Mohrenstraße 39, 10117 Berlin, Germany

[2]   Max Born Institute for Nonlinear Optics and Short Pulse Spectroscopy, Max-Born-Straße 2A, 12489 Berlin, Germany

[3]   Max-Planck-Institut für Physik komplexer Systeme, 01187 Dresden, Germany

[4]   Institut für Festkörpertheorie und -optik, Friedrich-Schiller-Universität, 07743 Jena, Germany

[5]   CEA-DAM, DIF, 91297 Arpajon, France

[6]   Optoelectronics Research Centre, Tampere University of Technology, 33101 Tampere, Finland

No. 1453
Berlin 2009

WIAS

Abstract

A plasma induced temporal break-up in filamentary propagation has recently been identified as one of the key events in the temporal self-compression of femtosecond laser pulses. An analysis of the Nonlinear Schrödinger Equation coupled to a noninstantaneous plasma response yields a set of stationary states. This analysis clearly indicates that the emergence of double-hump, characteristically asymmetric temporal on-axis intensity profiles in regimes where plasma defocusing saturates the optical collapse caused by Kerr self-focusing is an inherent property of the underlying dynamical model.

1   Introduction

Temporal compression of pulsed femtosecond laser beams within optical filaments provides a remarkably simple mechanism for the generation of ultrashort few-cycle pulses, in a wide spectral range from the mid infrared up to deep ultraviolet wavelengths [1, 2, 3, 4, 5]. One of the most outstanding features is the possibility to obtain temporally self-compressed pulses without any need for an external dispersion compensation scheme, indicating that the underlying compression mechanism differs from traditional laser pulse compression schemes [6, 7]. The self-compression process has been analyzed to occur in three steps [8], involving an initial plasma-induced pulse break-up, isolation of one of the fragments and subsequent compression of the latter upon further propagation. In contrast to previous explanations (see, e.g., [11, 9, 10]) that involved a complex interplay of numerous linear and nonlinear effects, it has been shown that self-compression can already occur due to diffraction, Kerr self-focusing and plasma induced self-defocusing. These three spatial effects completely suffice for an efficient on-axis compression of an isolated pulse [8, 12]. Within this scheme, a plasma induced temporal break-up, causing the intermittent occurrence of asymmetric double-hump field configurations, is essential for few-cycle pulse generation in laser filaments. Similar break-ups have been reported before, and they have typically been explained by an interplay of group dispersion and Kerr nonlinearity [13, 14]. In filaments, it has been shown that pulse splitting can also be promoted by the interplay of dispersion, multiphoton absorption, and the Kerr-nonlinearity, resulting in the formation of conical waves or X-waves [15, 16]. However, we find that there is a third previously unreported scenario that may give rise to pulse splitting. This scenario is dominated by spatial effects and manages without any dispersive coupling of temporal slices of the pulse. While pulse splitting in filaments has previously often been considered a compromising situation, the spa-

tially dominated scenario is found as the key step to initiate pulse self-compression in filaments.

In the following we present a detailed analysis of the origin of this characteristic asymmetric pulse break-up. Performing numerical simulations of the Nonlinear Schrödinger Equation (NLSE) coupled to an evolution equation for the electron density, we show that the pulse break-up dynamics in the efficiently ionized zone is already inherent in the interplay of only the above-mentioned three spatial effects. We analyze the double-hump on-axis temporal intensity distributions observed in the nonlinear focal region where plasma defocusing saturates the Kerr-based optical collapse. In this analysis we derive stationary state solutions directly from the Nonlinear Schrödinger Equation. It turns out that the local minimum between the sub-pulses of the characteristic double-hump solutions are located near the instant where the conserved power profile of the pulse has its maximum, i.e., at zero temporal delay. Regarding the power dependence of Kerr self-focusing, this behavior seems counterintuitive and is therefore further investigated using a time dependent variational approach that allows a prediction on the exact position of the local minimum.

2   Plasma induced pulse breaking in numerical simulations

In our simulations, we restrict ourselves to modeling spatial effects only. This disregards dissipative terms and energy exchange between adjacent temporal slices, thereby ensuring that these effects do not contribute to the observed temporal breakup. Treatment of this scenario in a full simulation provides qualitatively identical results [8]. Compared to the full model equations [11], the interplay between Kerr-type self-focusing and plasma defocusing therefore represents the primary dynamic effect during filament formation in gases. The propagation equation of this reduced model is expressed by the NLSE coupled to an evolution equation for the electron density [17]. Expressed in cylindrical coordinates (r, t) and in the reference frame moving with group velocity, the propagation equation for the slowly-varying envelope of complex optical field $\mathcal{E}(r, z, t)$ reads as

$$\partial_z \mathcal{E} = \frac{i}{2k_0 r}\partial_r r \partial_r \mathcal{E} + i\frac{\omega_0}{c}n_2|\mathcal{E}|^2\mathcal{E} - i\frac{1}{2n_0\rho_{\mathrm{c}}}\frac{\omega_0}{c}\rho(I)\mathcal{E}, \tag{1}$$

where z is the propagation length. The optical field envelope $\mathcal{E}$ is normalized such that the intensity is $I = |\mathcal{E}|^2$. The transverse Laplacian models the diffraction effects taking place in the transverse plane, with the radial distance from the optical axis given by $r = \sqrt{x^2 + y^2}$. The remaining terms on the right-hand side account for nonlinear self-focusing related to the Kerr effect and for plasma defocusing induced by an electron plasma with density ρ. The laser carrier frequency is given by ω_0 and related to the center wavelength via $\lambda_0 = 2\pi/k_0 = 2\pi c/\omega_0 = 800\,\mathrm{nm}$.
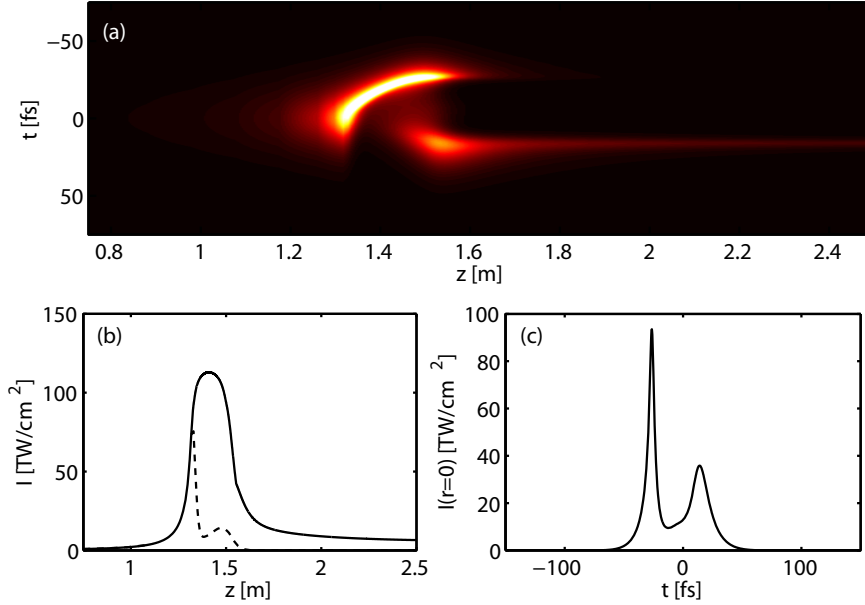
2

Figure 1: (a) Evolution of the on-axis temporal profile along z. As soon as plasma defocusing has saturated the optical collapse, a characteristic temporal break-up occurs. (b) Evolution of the peak intensity (solid line) and the on-axis intensity at zero delay (dashed line). (c) On-axis temporal distribution at $z = 1.55\,\mathrm{m}$ exhibiting a typical double hump structure.

$n_2 = 10^{-23}\mathrm{m}^2/\mathrm{W}$ is the nonlinear refractive index for argon at atmospheric pressure. The wavelength-dependent critical plasma density is calculated from the Drude model according to $\rho_c \equiv \omega_0^2 m_e \epsilon_0 / q_e^2$, where q_e and m_e are electron charge and mass, respectively, ϵ_0 is the dielectric constant, c the speed of light, and ρ_{nt} denotes the neutral density at atmospheric pressure. Neglecting recombination and collisional ionization, the time evolution of electron density is given by [18]

$$\rho(I) = \rho_{\mathrm{nt}} \left(1 - \exp\left(-\int_{-\infty}^{t} dt' W[I(t')] \right) \right), \qquad (2)$$

where plasma generation is driven by the ionization rate $W[I]$, which is suitably described by Perelomov-Popov-Terent'ev (PPT) theory [19]. For the numerical simulations and the analytical discussion, we use data for argon [11] at atmospheric pressure as parameters. As initial conditions for the numerical simulations, we impose a Gaussian spatio-temporal distribution for the photon density, with a pulse duration $t_p = 38\,\mathrm{fs}$ and beam waist $w_0 = 2.5\,\mathrm{mm}$. The input energy is $E_{\mathrm{in}} = 1\,\mathrm{mJ}$, corresponding to a peak input power of $P = 2P_{\mathrm{cr}}$, where $P_{\mathrm{cr}} \approx \lambda^2/2\pi n_2$ is the critical power for Kerr self-focusing. The beam is focused into the medium with an $f = 1.5\,\mathrm{m}$ lens. As no exchange of energy between time slices and no losses are considered, the optical power $P(t,z) = 2\pi \int_0^\infty r dr |\mathcal{E}(t,r,z)|^2$ is conserved along
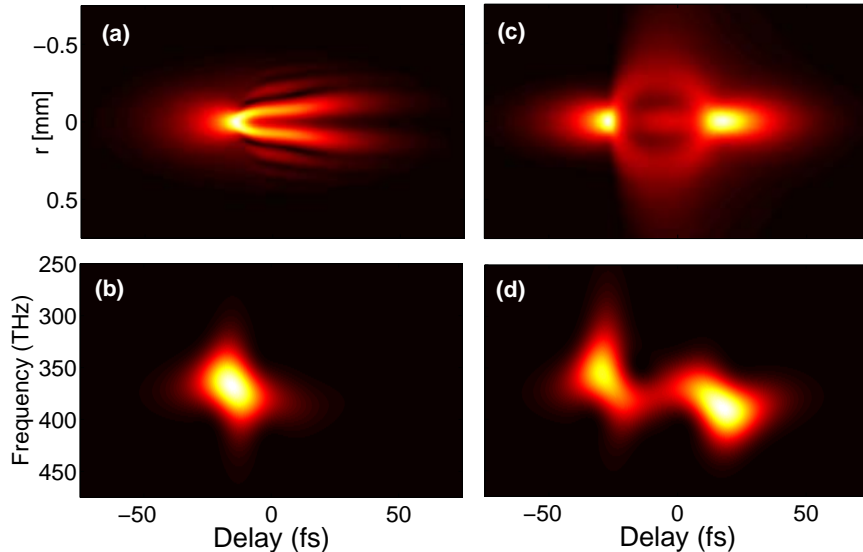
3

Figure 2: (a) Intensity distribution in the (r, t)-plane as plasma defocusing initiates the pulse break-up at $z = 1.37$ m. (b) Corresponding spectrogram. (c) Intensity distribution of the split pulse at $z = 1.55$ m in the (r, t)-plane. (d) Corresponding spectrogram.

propagation, i.e., $\partial_z P(t, z) \equiv 0$. The evolution of the on-axis intensity depicted in Fig. 1(a) reveals the crucial role of a plasma mediated temporal break-up for an efficient temporal compression induced by local contraction of the spatial beam profile, which has been termed self-pinching in Ref. [8]. In this process, filamentary compression undergoes two distinct phases. Initially, while z approaches the nonlinear focus, a dominant leading peak is observed. When the trailing part of the pulse refocuses in the efficiently ionized zone ($\rho_{max} \approx 5 \times 10^{16}$ cm^{-3}) a double-spiked structure emerges. Subsequently, only one of the emerging peaks survives and experiences further pulse shaping in the filamentary channel. The pulse breaking is initiated when plasma defocusing starts to saturate the optical collapse (see the evolution of the peak intensity in Fig. 1(b), solid line). Figure 2(a) depicts the intensity distribution in the (t, r) plane at $z = 1.37$ m, clearly revealing defocusing of the trailing part into a system of rings. The corresponding XFROG spectrogram [11] of the on-axis intensity profile [Fig. 2(b)], calculated with a 10 fs Gaussian reference pulse, exhibits an inclination due to the generation of red and blue frequencies in the leading and trailing edge of the pulse, respectively. Upon further propagation the rear part of this system of spatial rings merges during a refocusing stage at $z = 1.55$ m, and a blue-shifted trailing subpulse is generated [Figs. 2(c) and (d)]. The on-axis temporal profile of this strongly asymmetric temporal distribution depicted in Fig. 1(c) shows a characteristic double-hump configuration with a local minimum at zero delay. In the simulations, one can track the origin of this minimum to the fact that defocusing

4

prevails at zero delay. Therefore, the energy contained in the spatial rings at zero delay is not transferred back to the optical axis [dashed line in Fig. 1(b)]. From the spectrogram representation [Fig. 2(d)] of the split pulse, it becomes obvious that the trailing subpulse is blue-shifted with respect to the leading pulse. This spectro-temporal split is a characteristic feature for filamentary propagation [20, 21, 22], and it is important to note that this split is already fully explicable within the framework of the reduced model equation that incorporates only spatial effects.

3 Stationary states of the Nonlinear Schrödinger Equation with plasma response

At first sight, the emergence of the central minimum and the resulting double-hump temporal shapes may appear as a somewhat arbitrary intermediate stage in the pulse shaping process. For a clarification of the role of these characteristic pulse shapes which tend to appear when plasma defocusing saturates Kerr-driven optical collapse, we search for field configurations representing stationary states. These stationary spatio-temporal field distributions maintain a balance between competing nonlinear effects in every temporal point. The following analysis circumvents the limiting constraint of a fixed Gaussian radial shape, which has to be imposed in the time-dependent variational approach carried out in [8]. To further facilitate the calculation of stationary states to the evolution equation (1), for the ionization rate we use the multiphoton description $W[I] = \sigma_{N_*}|\mathcal{E}|^{2N^*}$. Here, σ_{N^*} is the cross-section for N^*-photon ionization [24]. As the relevant intensity level in argon filaments is well above the validity of a perturbative multiphoton description, the numerical value of $\sigma_{N^*} = 1.94 \times 10^{-74}\,\text{cm}^{2N^*}\text{W}^{-N^*}$ and $N^* = 6.13$ are determined by a local fit to the ionization rate given by PPT theory. As our model completely neglects dispersion, the time variable can be regarded as a parameter. Hence the most general ansatz for the stationary state reads as

$$\mathcal{E} = T(r,t)\exp i\mu(t)z, \tag{3}$$

where we explicitly allow a time-dependence of the propagation constant μ. Substituting this into the dynamical equation (1) yields the following nonlinear differential equation,

$$0 = \frac{1}{2k_0 r}\partial_r r\partial_r T + \frac{\omega_0}{c}n_2 T^3 - \frac{1}{2n_0\rho_c}\frac{\omega_0}{c}\rho T - \mu(t)T. \tag{4}$$

Any solution T of this equation depends on the specific choice of $\mu(t)$, as does the conserved optical power $P = 2\pi \int_0^\infty rdr T^2$, except for vanishing plasma density $\rho \equiv 0$. For the latter plasma-free case, the solution of (4) corresponds to the spatial Townes soliton [25] with an optical power $P'_{\text{cr}} \approx 11.69\lambda^2/(8\pi^2 n_2)$, independent of the chosen value of μ. Note that the optical power of the Townes soliton slightly differs from the usual definition of the critical power $P_{\text{cr}} = \lambda^2/(2\pi n_2)$, with $P_{\text{cr}}/P'_{\text{cr}} \approx 1.075$. In the presence of plasma, the general solution of (4) requires introduction of a cut-off time $-t_*$, imposing $P(t) < P'_{\text{cr}}$ for $t < -t_*$ similar to the variational analysis in
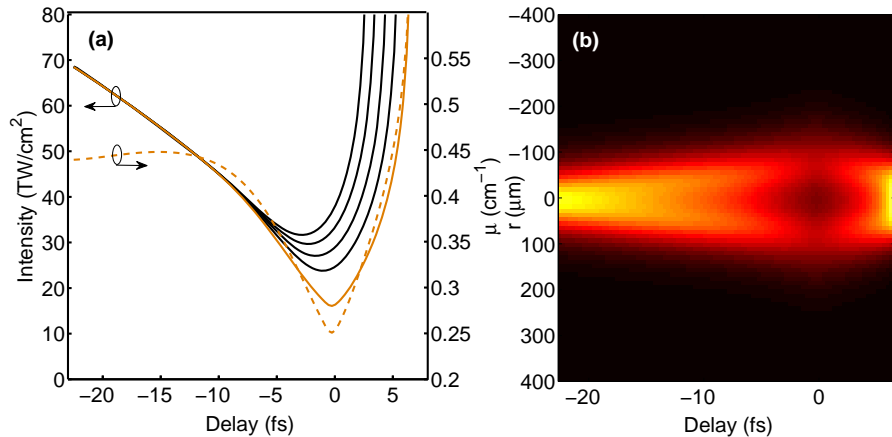
5

Figure 3: (a) On-axis temporal intensity profiles (solid lines) and propagation constant $\mu(t)$ corresponding to the orange curve(dashed line) of steady state solutions, obtained by solving Eq. (4), imposing a Gaussian power profile. (b) depicts the spatio-temporal representation of the curve marked in orange. Nontrivial stationary solutions only exist within the time-window $-t_* \leq t \leq t_*$ ($t_* \approx 22.4\,\text{fs}$).

[8]. With this constraint, Kerr self-focusing cannot compensate for linear diffraction at $t < -t_*$, and neither can a nontrivial stationary state exist. The solution at $t = -t_*$ itself radially coincides with the Townes soliton, as we assume $\rho \equiv 0$ at this very instant. Imposing a Gaussian power profile $P = P_{\text{in}} \exp\left(-2t^2/t_p^2\right)$ leads to $t_* = \sqrt{\ln\sqrt{P_{\text{in}}/P'_{\text{cr}}}}$. In order to obtain those functions $\mu(t)$ that give rise to stationary solutions with a conserved Gaussian power profile, we use a standard trust-region method [23] for nonlinear optimization in MatLab. We yield a continuum of stationary states, the on-axis intensity profiles of which are depicted in Fig. 3(a). We also supplement the propagation constant $\mu(t)$ of the solution represented by the orange curve in Fig. 3(a). The on-axis profiles feature the same characteristic double-hump temporal structure as in the numerical simulations. A similar analysis on time-dependent steady-state solutions was carried out earlier in [27, 26], however, with no prediction on pulse break-up. The intensity distribution in the (t, r) plane shown in Fig. 3(b) demonstrates that the plasma nonlinearity acts to defocus the temporal slices around zero delay into a spatial ring as was also observed in the simulations [cf. Figs. 2(a) and (c)]. In summary, evaluation of stationary solutions of (1) provides remarkable accurate predictions for the on-axis temporal profile and pulse breaking, occurring in a regime where plasma defocusing balances Kerr self-focusing.

4 Variational analysis of collapse saturation

Both, the numerical simulations as well as the stationary states calculated directly from the NLSE confirm that the emerging double-hump intensity distributions are defocused around zero delay. These time-slices actually contain the highest optical energy. As the strength of Kerr self-focusing is related to the optical power rather than intensity, this behaviour may be considered counterintuitive. In the following, we scrutinize the position of the local minimum in the double hump structure. This minimum is generally observed to occur when the competing nonlinear effects balance each other at any instant. In a time-dependent variational approach [18, 28], this condition gives rise to the nonlinear integral equation

$$
\begin{aligned}
0 \;=\; & 1 - \frac{P(t)}{P_{\text{cr}}} + \kappa P^2(t) \\
& \times \int_{-\infty}^{t} dt' \frac{I^{N^*+1}(t')}{P(t')} \frac{1}{\left(I(t) + N^* I(t') \frac{P(t)}{P(t')}\right)^2}
\end{aligned}
\tag{5}
$$

for the on-axis intensity profile $I(t)$ of the stationary state. A continuum of solutions of (5) is shown in Fig. 4(a). Quite remarkably, these solutions are in good agreement with the solutions derived directly from the NLSE, showing the characteristic double-hump structure with a minimum around zero delay. In order to calculate the exact position of the minimum we differentiate (5) with respect to the retarded time variable t and subsequently set $\partial/\partial t\, I(t) = 0$ in the resulting expression. This yields the nonlinear integral equation

$$
\begin{aligned}
0 \;=\; & \dot{G}(t) I^2(t) + \frac{\kappa}{(1+N^*)^2} \frac{I^{N^*+1}(t)}{P(t)} \\
& - 2\kappa N^* \frac{\dot{P}(t)}{I(t)} \int_{-\infty}^{t} dt'\, K[t, t', I(t), I(t')]
\end{aligned}
\tag{6}
$$

with $\kappa = k_0^2 N^* \sigma_{N^*} \rho_{\text{nt}}/\pi \rho_{\text{c}}$ and

$$
G(t) = \frac{1 - P(t)/P_{cr}}{P^2(t)}
$$

and an integral kernel

$$
K[t, t', I(t), I(t')] = \frac{I^{N^*+2}(t')}{P^2(t')\left(1 + N^* \frac{I(t')P(t)}{I(t)P(t')}\right)^3},
$$

in which $P_{\text{cr}} = \lambda_0^2/(2\pi n_0 n_2)$. The nonlinear integral equation (6) is basically a generalization of a Volterra-Urysohn integral equation [29], with a kernel depending not only on $I(t')$ but also on $I(t)$. Combining a Clenshaw-Curtis quadrature scheme
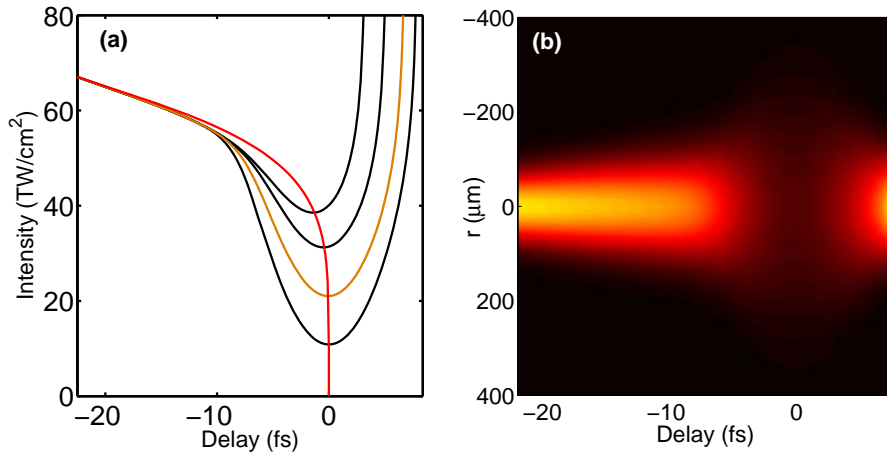
Figure 4: (a) On-axis intensity profile of steady state solutions calculated from a variational approach according to Eq. (5). The solid red line represents a solution to Eq. (6), indicating the position of the local minimum. (b) depicts the spatio-temporal representation of the curve marked in orange.

for the integral term of (6) with a Chebyshev expansion of the unknown function $I(t)$ yields a set of nonlinear equations for the expansion coefficient [30], which are solved utilizing standard algorithms for nonlinear optimization in Matlab [23]. The solution of this equation is depicted by the solid red line in Fig. 4(a). Moving along this line towards positive times, the local minimum of the solution appears more pronounced.

This indicates that the pulse splitting mechanism works most effectively in the vicinity of zero delay. Our analysis therefore explains the peculiarity of the split preferentially occurring at the instant of maximum power inside the pulse. Although the variational approach provides a good estimate on the exact on-axis temporal profile of the steady states shown in Fig. 3(a), one can certainly not expect an exact coincidence with the exact solutions, as the variational approach imposes a fixed Gaussian radial shape of the pulse as shown in Fig. 4(b). In particular, the simplifying assumption of a Gaussian spatial profile neglects the fact that plasma defocusing actually gives rise to the formation of spatial rings. Nevertheless, our analysis corroborates a tendency for self-pinching and pulse break-up.

5   Conclusions

Starting from an independently obtained observation of filamentary pulse-breakup both in numerical simulations and experimental investigations, we investigated stationary states of the NLSE coupled to a noninstataneous plasma response. The resulting solutions provide a remarkable prediction for the plasma-induced break-up

scenario in the strongly ionized filament channel. The quality of the exact solutions compares favorably to stationary solution obtained in [8] from a time dependent variational approach. In particular, the position of the local minimum separating the individual sub-pulses is directly obtained from a nonlinear integral equation. Both, the exact and the variational approach of deriving stationary solutions to the NLSE corroborates the temporal break-up observed in the numerical simulations and the emergence of local minima of the intensity profile around zero delay. In summary, we conclude that when plasma defocusing saturates the optical breakdown, our assumption of emerging steady state profiles offers deep insight on the dynamical behavior and underlying mechanisms of a physical system that was previously only accessible in detailed numerical simulations.

References

[1] C. P. Hauri, R. B. Lopez-Martens, C. I. Blaga, K. D. Schultz, J. Cryan, R. Chirla, P. Colosimo, G. Doumy, A. M. March, C. Roedig, E. Sistrunk, J. Tate, J. Wheeler, L. R. DiMauro, E. P. Power, Opt. Lett. **32**, 868 (2007).

[2] L. Bergé, Opt. Express **16**, 21529 (2008).

[3] C. P. Hauri, W. Kornelis, F. W. Helbing, A. Heinrich, A. Couairon, A. Mysyrowicz, J. Biegert, U. Keller, Appl. Phys. B **79**, 673 (2004).

[4] G. Stibenz, N. Zhavoronkov, G. Steinmeyer, Opt. Lett. **31**, 274 (2006).

[5] L. Bergé, S. Skupin, Opt. Lett. **33** 750 (2008).

[6] E. B. Treacy, IEEE J. Quantum Electron. **5**, 454 (1969).

[7] C. V. Shank, R. L. Fork, R. Yen, and R. H. Stolen, and W. J. Tomlinson, Appl. Phys. Lett. **40**, 761 (1982).

[8] C. Brée, A. Demircan, S. Skupin, L. Bergé, and G. Steinmeyer, Opt. Express. **17**, 16429 (2009).

[9] A. Couairon, M. Franco, A. Mysyrowicz, J. Biegert, and U. Keller, Opt. Lett. **30**, 2657–2659 (2005).

[10] L. T. Vuong, R. B. Lopez-Martens, C. P. Hauri, and A. L. Gaeta, Opt. Express **16**, 390–401 (2008).

[11] S. Skupin, G. Stibenz, L. Bergé, F. Lederer, T. Sokollik, M. Schnuerer, N. Zhavoronkov, and G. Steinmeyer, Phys. Rev. E **74**, 056604 (2006).

[12] C. Brée, A. Demircan, and G. Steinmeyer, Laser Phys. **19**, 330 (2009).

[13] N. A. Zharova, A. G. Litvak, T. A. Petrova, A. M. Sergeev, and A. D. Yunakovskii, JETP Lett. **44**, 13 (1986).

[14] A. A. Zozyula, S. A. Diddams, A. G. Van Engen, and T. S. Clement, Phys. Rev. Lett. **82**, 1430 (1999).

[15] D. Faccio, A. Matijosius, A. Dubietis, R. Piskarskas, A. Varanvičius, E. Gaizauskas, A. Piskarskas, A. Couairon, and P. Di Trapani, Phys. Rev. E **72**, 037601 (2005).

[16] M. A. Porras, A. Parola, D. Faccio, A. Couairon, and P. Di Trapani, Phys. Rev. A **76**, 011803(R) (2007).

[17] L. Bergé and A. Couairon, Phys. Rev. Lett. **86**, 1003 (2001).

[18] L. Berge, S. Skupin, R. Nuter, J. Kasparian, and J. P. Wolf, Rep. Prog. Phys. **65**, 026611 (2007).

[19] A. M. Perelomov, V. S. Popov, and M. V. Terent'ev, Sov. Phys. JETP **23**, 924 (1966).

[20] S. L. Chin, Y. Chen, O. Kosareva, V. P. Kandidov and F. Théberge, Laser Phys. **18**, 962 (2008).

[21] V. P. Kandidov, S. A. Shlenov, O. G. Kosareva, Quantum Electronics **39**, 205 (2009).

[22] M. Mlejnek, E. M. Wright, and J. V. Moloney, Opt. Lett. **23**, 382 (1998).

[23] T. F. Coleman and Y. Li, SIAM Journal on Optimization **6**, 418 (1996).

[24] C. Brée, A. Demircan, and G. Steinmeyer, accepted for publication in IEEE JQE

[25] R. Y. Chiao, E. Garmire, and C. H. Townes, Phys. Rev. Lett. **13**, 479 (1964).

[26] E. Esarey, P. Sprangle, J. Krall, and A. Ting, IEEE Journal Quantum Electron. **33**, 1879 (1997).

[27] S. Henz and J. Herrmann, Phys. Rev. E **53**, 4092 (1996).

[28] L. Bergé and A. Couairon, Phys. Plasmas **7**, 210 (2000).

[29] M. A. Darwish, Appl. Math. Comput. **136**, 93–98 (2003).

[30] C. W. Clenshaw and A. R. Curtis, Numer. Math. **2**, 197–205 (1960).